

Rolling and sliding of a nanoparticle between two planes: Tribological regimes and control of friction

Mykhaylo Evstigneev* and Peter Reimann
Universität Bielefeld, Fakultät für Physik, 33615 Bielefeld, Germany

The motion of a cylindrical crystalline nanoparticle sandwiched between two crystalline planes, one stationary and the other pulled at a constant velocity and pressed down by a normal load, is considered theoretically using a planar model. The results of our model calculations show that, depending on load and velocity, the nanoparticle can be either rolling or sliding. At sufficiently high normal loads, several sliding states characterized by different friction forces can coexist, corresponding to different orientations of the nanoparticle, and allowing one to have low or high friction at the same pulling velocity and normal load.

PACS numbers: 46.55.+d, 62.20.Qp, 68.35.Af, 07.79.Sp

I. INTRODUCTION

Because of its great importance for nanotechnological applications, control of friction at the nanoscale is a hot topic of current research. While conventional lubricants cannot be applied for this purpose, research efforts have been guided by the vision of Richard Feynman that the nanobearings can “run dry”¹. It has been shown that decreasing the normal load² or pulling velocity³, as well as normal load actuation⁴ can lead to a dramatic friction reduction. A mechanism of friction control particularly pertinent to our present work is the so-called structural lubricity, or superlubricity^{5–13}, arising due to the structural incommensurability of the two contacting surfaces. More precisely, each atom of the sliding surface feels the force generated by the periodically arranged atoms of the substrate, so that the total friction force is the sum of the forces felt by each atom of the slider. If the slider and the substrate are incommensurate, these forces add up randomly, resulting in nearly frictionless sliding. The phenomenon of superlubricity has been observed experimentally^{7,11–13}. On the other hand, it has been demonstrated by means of molecular dynamics simulations¹⁴, as well as stochastic modelling and experiment¹⁵ that a flat nanoobject (e.g. a graphite flake) in contact with the surface quickly reorients itself into the “commensurate” state of high friction, even though the initial orientation may be the superlubric one.

Finally, one can influence the friction forces by using the rolling motion of round nanoparticles in between the surfaces^{16–21}. Nanoparticle rolling can be identified experimentally by making a small indentation on its surface with a sharp tip of an atomic force microscope and subsequent localization of this mark after the manipulation¹⁹. Alternatively, for a highly symmetric nanoparticle, such as a carbon nanotube, a rolling regime can be identified from the characteristic periodicity of the time-dependent friction force – in the rolling state, this periodicity is proportional to the circumference of the nanoparticle^{20,21}.

In this paper, we consider the motion of a cylindrical nanoparticle sandwiched between two planes, see Fig. 1. Because of the unavoidable deviations from a perfect ro-

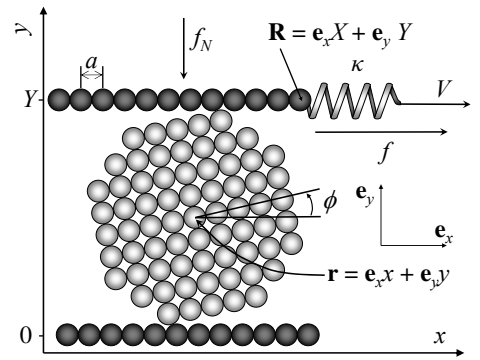


FIG. 1: Schematic illustration of the system: a nanoparticle is sandwiched between the stationary lower plane and the upper plane pressed down by the normal load f_N and attached to a spring of stiffness κ , whose other end is pulled with the velocity V . The friction force f is deduced from the elastic deformation of the spring attached to the upper plane, cf. Eq. (2).

tational symmetry, the surface of the nanoparticle actually consists of facets characterized by different lattice constants, and hence by different commensurabilities with both planes²¹. Based on a simple model described in Section II, we show in Section III that the nanoparticle can be stabilized in several friction states, namely, rolling friction and different sliding regimes that can be realized depending on which facets of the nanoparticle are in contact with the upper and lower surface. These results are summarized in a state diagram showing the stability regions of different friction states depending on the two experimental control parameters – normal load and pulling velocity. The state diagram contains a region, where sliding friction regimes characterized by commensurate contact (high friction forces) and incommensurate contact (low friction forces) of the nanoparticle coexist. We propose a friction switching scenario, allowing one to realize either low or high friction forces at the same

pulling velocity and normal load.

II. THE MODEL

A. Equations of motion

We consider a crystalline nanoparticle, approximating as close as possible a round shape of some preset radius, see Fig. 1. Unlike the symmetric fullerene-like molecules with equivalent ‘facets’ studied in Refs. 16–18, in our system, the facets have different number of atoms and different commensurability with the planes, see Fig. 1, so that, depending on which facets are in contact with the planes, different friction regimes may be realized. While our model system from Fig. 1 is two-dimensional, the main results immediately carry over to some three-dimensional objects, such as nanorods. We henceforth consider a single particle, expecting analogous findings for the case of many particles, provided they are sufficiently dilute.

The overall geometric configuration of the system is completely determined by the nanoparticle’s center of mass $\mathbf{r} = x\mathbf{e}_x + y\mathbf{e}_y$, its rotation angle ϕ , and the position $\mathbf{R} = X\mathbf{e}_x + Y\mathbf{e}_y$ of some reference atom from the top plane, which we assume to be horizontal at all times; here $\mathbf{e}_{x,y}$ are the unit vectors in the x - and y -direction. If the nanoparticle and the planes could be viewed as rigid bodies, the equations of motion for the generalized coordinates $(\mathbf{r}, \phi, \mathbf{R})$ would be derivable from the Lagrangian

$$L(\mathbf{r}, \phi, \mathbf{R}, \dot{\mathbf{r}}, \dot{\phi}, \dot{\mathbf{R}}) = \frac{m\dot{\mathbf{r}}^2}{2} + \frac{I\dot{\phi}^2}{2} + \frac{M\dot{\mathbf{R}}^2}{2} - U_B(\mathbf{r}, \phi) - U_T(\mathbf{R} - \mathbf{r}, \phi) - \frac{\kappa(X - Vt)^2}{2} + f_N Y, \quad (1)$$

where the first two terms represent the translational and rotational kinetic energy of the nanoparticle with mass m and moment of inertia I ; the third term describes the kinetic energy of the upper plane of mass M ; the fourth and the fifth terms correspond to the interaction between the nanoparticle and the bottom and top planes, respectively; the last two terms correspond to the energy of elastic deformation of the spring of stiffness κ whose other end is pulled at the constant velocity V , and the energy of the upper plane produced by the normal load. Therefore, the elastic force generated by the spring is equal in magnitude to the instantaneous friction force

$$f = -\kappa(X - Vt). \quad (2)$$

We furthermore assume that the separation between the two planes – the nanoparticle’s diameter – is sufficiently large, so that the interaction energy between them is negligible.

In reality, the atoms of the nanoparticle and the planes are not rigidly coupled to each other, and their motion affects the motion of the global coordinates \mathbf{r} , ϕ , and \mathbf{R} . If the time scales of the overall nanoparticle motion is much

slower than the time scale of individual atoms, the interaction between the global degrees of freedom, \mathbf{r} , ϕ , \mathbf{R} , and those of atoms composing the nanoparticle, both planes, and the spring can be approximately taken into account by means of the following three modifications of the equations of motion generated by the Lagrangian (1)²²:

(i) renormalization of the forces and torques acting on the relevant coordinates \mathbf{r} , ϕ , and \mathbf{R} ;

(ii) introduction of velocity-dependent dissipation forces describing the effect of energy loss from the global degrees of freedom \mathbf{r} , ϕ , and \mathbf{R} into the atomistic degrees of freedom of the nanoparticle, both planes, and the spring attached to the upper plane;

(iii) introduction of noise corresponding to the inverse process of energy transfer from random atomic vibrations into the global degrees of freedom.

The effect (i) is accounted for by reinterpreting the energies $U_{B,T}$ as free energies. The dissipative forces (ii) due to the internal degrees of freedom of the nanoparticle and the planes can be derived from the dissipation function²³,

$$\Phi(\mathbf{r}, \phi, \mathbf{R}, \dot{\mathbf{r}}, \dot{\phi}, \dot{\mathbf{R}}) = \frac{1}{2} \sum_{q,q'} \eta_{qq'}(\mathbf{r}, \phi, \mathbf{R}) \dot{q}\dot{q}', \quad (3)$$

where the generalized coordinate indices q, q' run over the values (x, y, ϕ, X, Y) , and the dissipation coefficients are symmetric,

$$\eta_{qq'} = \eta_{q'q}. \quad (4)$$

These forces are written as velocity derivatives of the dissipation function, $f_q^{diss} = -\partial\Phi/\partial\dot{q} = -\sum_{q'} \eta_{qq'} \dot{q}'$. Similarly, an additional dissipative force on the upper plane arises due to the internal degrees of freedom of the spring: $f_{spring}^{diss} = -\eta_S(\dot{\mathbf{R}} - V\mathbf{e}_x)$. This additional dissipation channel is not present in the dissipation function (3), because the position Vt of the pulled end of the spring is not a generalized coordinate in the Lagrangian (1); therefore, the dissipative force f_{spring}^{diss} should be included ‘‘by hand’’. Finally, we account for the noise effect (iii) by adding suitably chosen Gaussian white noises to the right-hand side of the equations of motion:

$$\begin{aligned} m\ddot{\mathbf{r}} &= -\nabla[U_B(\mathbf{r}, \phi) - U_T(\mathbf{R} - \mathbf{r}, \phi)] \\ &\quad -\eta_{\mathbf{r}\mathbf{r}}\dot{\mathbf{r}} - \eta_{\mathbf{r}\phi}\dot{\phi} - \eta_{\mathbf{r}\mathbf{R}}\dot{\mathbf{R}} + \xi_{\mathbf{r}}(t), \\ I\ddot{\phi} &= -\frac{\partial[U_B(\mathbf{r}, \phi) + U_T(\mathbf{R} - \mathbf{r}, \phi)]}{\partial\phi} \\ &\quad -\eta_{\phi\mathbf{r}}\dot{\mathbf{r}} - \eta_{\phi\phi}\dot{\phi} - \eta_{\phi\mathbf{R}}\dot{\mathbf{R}} + \xi_{\phi}(t), \\ M\ddot{\mathbf{R}} &= -\nabla U_T(\mathbf{R} - \mathbf{r}, \phi) - \kappa(X - Vt)\mathbf{e}_x - f_N\mathbf{e}_y \\ &\quad -\eta_{\mathbf{R}\mathbf{r}}\dot{\mathbf{r}} - \eta_{\mathbf{R}\phi}\dot{\phi} - \eta_{\mathbf{R}\mathbf{R}}\dot{\mathbf{R}} - \eta_S(\dot{\mathbf{R}} - V\mathbf{e}_x) \\ &\quad + \xi_{\mathbf{R}}(t) + \xi_S(t). \end{aligned} \quad (5)$$

Here, $\eta_{\mathbf{r}\mathbf{r}}$ is a tensor with components $\eta_{xx}, \eta_{xy}, \eta_{yx} = \eta_{xy}, \eta_{yy}$, with similar definitions for $\eta_{\mathbf{r}\mathbf{R}}$ and $\eta_{\mathbf{R}\mathbf{R}}$. Also, $\eta_{\mathbf{r}\phi}$ and $\eta_{\mathbf{R}\phi}$ are vectors, e.g. $\eta_{\mathbf{r}\phi} = \eta_{x\phi}\mathbf{e}_x + \eta_{y\phi}\mathbf{e}_y$ with a similar definition for $\eta_{\mathbf{R}\phi}$, and $\eta_{\phi\mathbf{r}} = \eta_{\mathbf{r}\phi}^T$, $\eta_{\phi\mathbf{R}} = \eta_{\mathbf{R}\phi}^T$.

are the respective transposed vectors. The Gaussian white noises $\xi_q(t)$, $q = x, y, \phi, X, Y$ have zero mean and obey the fluctuation-dissipation theorem of the second kind, $\langle \xi_q(t)\xi_{q'}(t') \rangle = 2T\eta_{qq'}(\mathbf{r}, \phi, \mathbf{R})\delta(t' - t)$. The noise $\xi_S(t)$ due to the spring is uncorrelated with the noises $\xi_q(t)$ and its autocorrelation function is $\langle \xi_{S\alpha}(t)\xi_{S\beta}(t') \rangle = 2T\eta_S\delta_{\alpha\beta}\delta(t' - t)$, where α, β refer to the coordinates x, y .

B. Choice of the functional form for the potentials and dissipation coefficients

Having written down the general equations of motion (5) for the relevant coordinates, we should specify the functional forms of the potentials $U_{B,T}$, as well as the dissipation coefficients $\eta_{\mathbf{r}\mathbf{r}}$, $\eta_{\mathbf{r}\phi}$, etc. We consider the potentials first. For simplicity, we assume the upper and the lower planes to be equivalent, leading to

$$U_T(\mathbf{R} - \mathbf{r}, \phi + \pi) = U_B(\mathbf{r}, \phi) =: U(\mathbf{r}, \phi), \quad (6)$$

and leaving us with the necessity to determine the function $U(\mathbf{r}, \phi)$. This function should possess the symmetries

$$U(\mathbf{r}, \phi) = U(\mathbf{r} + a\mathbf{e}_x, \phi) = U(\mathbf{r}, \phi + 2\pi/N), \quad (7)$$

where a is the lattice constant of the plane, and N is an integer related to the rotational symmetry of the particle. For example, for a nanoparticle as sketched in Fig. 1, we have $N = 4$. There are many functions with the property (7). To make a physically motivated choice, we view the nanoparticle as a collection of periodically arranged ‘‘pseudoatoms’’, where each pseudoatom represents a group of closely arranged real atoms of the particle. In particular, if Fig. 1 depicts a cross-section of a nanorod, then each pseudoatom describes the cumulative effect of an atomic row along the axis perpendicular to the plane of the figure. The i th pseudoatom of the nanoparticle has the coordinate

$$\mathbf{r}_i(\mathbf{r}, \phi) = \mathbf{r} + d_i\mathbf{e}_i(\phi), \quad (8)$$

where $d_i = |\mathbf{r}_i - \mathbf{r}|$ is the rigidly fixed distance of the i th pseudoatom from the center of mass, and $\mathbf{e}_i(\phi) = \mathbf{e}_x \cos(\theta_i + \phi) + \mathbf{e}_y \sin(\theta_i + \phi)$ is the unit vector pointing from the center of mass to the i th pseudoatom. The constant angles θ_i are completely determined by the crystal structure of the nanoparticle.

The potential of interaction with the bottom plane is the sum of the respective interaction energies of all pseudoatoms

$$U(\mathbf{r}, \phi) = \sum_i u(\mathbf{r}_i(\mathbf{r}, \phi)). \quad (9)$$

The functions $u(\mathbf{r}) = u(\mathbf{r} + a\mathbf{e}_x)$ can be expanded into Fourier series in x with the expansion coefficients depending on the y -component of \mathbf{r} . Neglecting the second and higher harmonics, we employ the functional form

$$u(\mathbf{r}) = u_0(y) + u_1(y) \cos \frac{2\pi x}{a}. \quad (10)$$

To account for the possibility of adhesion, the zero-order term is taken to be the Lennard-Jones potential,

$$u_0(y) = \varepsilon \left((\sigma/y)^{12} - 2(\sigma/y)^6 \right), \quad (11)$$

where ε is the adhesion energy and σ the equilibrium separation from the surface.

The function $u_1(y)$ in Eq. (10) has the physical meaning of the corrugation amplitude of the potential (10) in the x -direction. We assume it to increase exponentially upon approaching the surface:

$$u_1(y) = \Delta U e^{-(y-\sigma)/\lambda}, \quad (12)$$

where ΔU is the corrugation at the equilibrium separation σ , and λ is the characteristic decay length.

With respect to the dissipation coefficients of the nanoparticle, we should distinguish between the contributions due to the bottom and the top planes. We assume that in the course of its translational and rotational motion, the total dissipative force on the nanoparticle is a sum of the respective contributions from all its pseudoatoms. That is, the motion of the i th pseudoatom with the velocity $\dot{\mathbf{r}}_i$ relative to the bottom plane results in the dissipative force $-\eta(\mathbf{r}_i)\dot{\mathbf{r}}_i$ on that pseudoatom. The expression for the dissipative force contribution from the top plane is similar, but with the dissipation coefficient $\eta(\mathbf{R} - \mathbf{r}_i)$ and the relative velocity $\dot{\mathbf{r}}_i - \dot{\mathbf{R}}$.

For simplicity, we assume isotropy of the damping coefficients $\eta(\mathbf{r}_i)$, which are treated as scalar functions of the position \mathbf{r}_i . We choose the following functional form:

$$\eta(\mathbf{r}_i) = \eta_0 e^{-(y_i - \sigma)/\xi}, \quad (13)$$

η_0 being the damping coefficient at the minimum of the Lennard-Jones potential (11), and ξ the decay length. Explicitly, the velocity of i th pseudoatom is expressed in terms of the generalized velocities $\dot{\mathbf{r}}$ and $\dot{\phi}$ as

$$\dot{\mathbf{r}}_i(\mathbf{r}, \phi) = \dot{\mathbf{r}} + d_i\mathbf{t}_i(\phi)\dot{\phi}, \quad (14)$$

where the tangential vector is

$$\mathbf{t}_i(\phi) = \frac{d\mathbf{e}_i(\phi)}{d\phi} = -\mathbf{e}_x \sin(\theta_i + \phi) + \mathbf{e}_y \cos(\theta_i + \phi). \quad (15)$$

The dissipative force due to the bottom plane is

$$\mathbf{f}_{diss}^B = - \sum_i \eta(\mathbf{r}_i)\dot{\mathbf{r}}_i = - \sum_i \eta(\mathbf{r}_i)\dot{\mathbf{r}} - \sum_i \eta(\mathbf{r}_i)d_i\mathbf{t}_i\dot{\phi}. \quad (16)$$

The dissipative force due to the top plane has a similar form, but with the velocity $\dot{\mathbf{r}}_i$ replaced with $\dot{\mathbf{r}}_i - \dot{\mathbf{R}}$ and $\eta(\mathbf{r}_i)$ with $\eta(\mathbf{R} - \mathbf{r}_i)$, that is

$$\mathbf{f}_{diss}^T = - \sum_i \eta(\mathbf{R} - \mathbf{r}_i)(\dot{\mathbf{r}} - \dot{\mathbf{R}}) - \sum_i \eta(\mathbf{R} - \mathbf{r}_i)d_i\mathbf{t}_i\dot{\phi}. \quad (17)$$

Summing all the contributions, we obtain:

$$\eta_{\mathbf{r}\mathbf{r}} = \sum_i [\eta(\mathbf{r}_i) + \eta(\mathbf{R} - \mathbf{r}_i)]\mathbf{I},$$

$$\begin{aligned}\eta_{\mathbf{r}\phi} &= \sum_i [\eta(\mathbf{r}_i) + \eta(\mathbf{R} - \mathbf{r}_i)] d_i \mathbf{t}_i, \\ \eta_{\mathbf{r}\mathbf{R}} &= - \sum_i \eta(\mathbf{R} - \mathbf{r}_i) \mathbf{I},\end{aligned}\quad (18)$$

where \mathbf{I} is a unit 2×2 tensor.

In view of the symmetry (4) of the dissipation coefficients, the second of these equations (18) uniquely fixes $\eta_{\phi\mathbf{r}} = \eta_{\mathbf{r}\phi}^T$. To determine the remaining coefficients $\eta_{\phi\phi}$ and $\eta_{\phi\mathbf{R}}$, we should consider the torque produced by the dissipative force as the nanoparticle rotates between both planes. The magnitude of this torque is $K_{diss} = - \sum_i d_i [\eta(\mathbf{r}_i) \dot{\mathbf{r}}_i + \eta(\mathbf{R} - \mathbf{r}_i) (\dot{\mathbf{r}}_i - \dot{\mathbf{R}})] \cdot \mathbf{t}_i$. Upon substitution of the expression (14) we find

$$\begin{aligned}\eta_{\phi\mathbf{R}} &= - \sum_i \eta(\mathbf{R} - \mathbf{r}_i) d_i \mathbf{t}_i^T, \\ \eta_{\phi\phi} &= \sum_i [\eta(\mathbf{r}_i) + \eta(\mathbf{R} - \mathbf{r}_i)] d_i^2.\end{aligned}\quad (19)$$

For the upper plane, we have from the symmetry (4) of the dissipation coefficients $\eta_{\mathbf{r}\mathbf{r}} = \eta_{\mathbf{R}\mathbf{R}}$ and $\eta_{\mathbf{R}\phi} = \eta_{\phi\mathbf{R}}^T$. The remaining tensor $\eta_{\mathbf{R}\mathbf{R}}$ describes the effect of energy dissipation of the upper plane into the internal degrees of freedom of the stationary nanoparticle and has the form:

$$\eta_{\mathbf{R}\mathbf{R}} = \sum_i \eta(\mathbf{R} - \mathbf{r}_i) \mathbf{I}.\quad (20)$$

C. Overdamped zero-temperature limit

It is difficult to estimate the dissipation coefficients from first principles, because the basic building block of our model – a pseudoatom – is a complex object consisting of many real atoms. It is not unreasonable to assume though that the dissipation coefficient of such a pseudoatom (and of the nanoparticle itself) can be many orders of magnitude higher than that of a true atom on a surface. Therefore, in our numerical calculations, we assume that the dissipation effects are much stronger than the inertia effects, allowing us to consider the overdamped limit by formally setting the nanoparticle's mass and moment of inertia to zero: $m = 0$, $I = 0$. Likewise, we assume that the spring attached to the upper plane is overdamped, allowing us to set $M = 0$. Finally, since the potential energies from Eq. (1) represent an effect of many atoms, noise effects can be assumed extremely small in comparison to the interaction forces and the normal load. Therefore, we neglect thermal noise by setting T to zero in the equations of motion (5), yielding

$$\begin{aligned}\eta_{\mathbf{r}\mathbf{r}} \dot{\mathbf{r}} + \eta_{\mathbf{r}\phi} \dot{\phi} + \eta_{\mathbf{r}\mathbf{R}} \dot{\mathbf{R}} &= \\ -\nabla[U(\mathbf{r}, \phi) - U(\mathbf{R} - \mathbf{r}, \phi + \pi)] &, \\ \eta_{\phi\mathbf{r}} \dot{\mathbf{r}} + \eta_{\phi\phi} \dot{\phi} + \eta_{\phi\mathbf{R}} \dot{\mathbf{R}} &= \\ \frac{\partial[U(\mathbf{r}, \phi) + U(\mathbf{R} - \mathbf{r}, \phi + \pi)]}{\partial\phi} &,\end{aligned}$$

$$\begin{aligned}\eta_{\mathbf{R}\mathbf{r}} \dot{\mathbf{r}} + \eta_{\mathbf{R}\phi} \dot{\phi} + \eta_{\mathbf{R}\mathbf{R}} \dot{\mathbf{R}} &= -\nabla U(\mathbf{R} - \mathbf{r}, \phi + \pi) \\ -\eta_S(\dot{\mathbf{R}} - V\mathbf{e}_x) - \kappa(X - Vt)\mathbf{e}_x - f_N\mathbf{e}_y &.\end{aligned}\quad (21)$$

These equations can be simplified even further if we consider a nanoparticle, which is symmetric with respect to rotations by π , as in Fig. 1. Due to this symmetry, and due to the equivalence of the upper and lower planes, we can state that there is a solution of Eqs. (21), for which

$$\mathbf{r} = \mathbf{R}/2\quad (22)$$

up to an addition of an integer multiple of the lattice constant a in the x -direction. This is verified by inspection of the first of the equations of motion (21), where substitution of the relation (22) renders the force in the right-hand side vanish. Considering the left-hand side, let us have a closer look at the damping coefficients from Eq. (18). Because our nanoparticle is symmetric with respect to rotations by π , for each pseudoatom at $\mathbf{r}_i = \mathbf{R}/2 + d_i\mathbf{e}_i$ there is a symmetric partner pseudoatom at $\mathbf{r}_k = \mathbf{R}/2 - d_i\mathbf{e}_i$. Then, comparison of the first and the third equations (18) yields $\eta_{\mathbf{r}\mathbf{r}} = -2\eta_{\mathbf{R}\mathbf{R}}$. Furthermore, since the tangential vectors (15) of the i th and the k th pseudoatoms are opposite to each other, $\mathbf{t}_k = -\mathbf{t}_i$, the sum in the second equation (18) vanishes, $\eta_{\mathbf{r}\phi} = 0$, automatically implying that $\eta_{\phi\mathbf{r}} = 0$. Then, the first equation (21) reduces to $\eta_{\mathbf{r}\mathbf{R}}(\dot{\mathbf{R}} - 2\dot{\mathbf{r}}) = 0$, implying Eq. (22). By numerically integrating the full set of equations (21), we have verified that the relation (22) is stable: for all initial conditions tried, the system eventually entered the regime with $\mathbf{r} = \mathbf{R}/2$. Therefore, computational effort can be reduced by roughly a factor of two by replacing five equations (21) with three equations of motion for ϕ , X , and Y :

$$\begin{aligned}\eta_{\phi\phi} \dot{\phi} + \eta_{\phi\mathbf{R}} \dot{\mathbf{R}} &= -2 \frac{\partial U(\mathbf{R}/2, \phi)}{\partial\phi}, \\ [\eta_S + \eta_{\mathbf{R}\mathbf{R}} + \eta_{\mathbf{R}\mathbf{r}}/2] \dot{\mathbf{R}} + \eta_{\mathbf{R}\phi} \dot{\phi} &= -\nabla U(\mathbf{R}/2, \phi) \\ + [\eta_S V - \kappa(X - Vt)] \mathbf{e}_x - f_N \mathbf{e}_y &.\end{aligned}\quad (23)$$

III. RESULTS AND DISCUSSION

A. Parameters and units

In all our numerical results below, we have chosen the lattice constant a as the unit of length, the adhesion energy ε as the unit of energy, and the ratio $\eta_0 a^2 / \varepsilon$ as the unit of time. This choice fixes the unit of force to ε/a , the unit of velocity to $\varepsilon/(a\eta_0)$, and the unit of spring constant to ε/a^2 . The value of the dissipation coefficient at the minimum of the potential (11) in these units is $\eta_0 = 1$, and, obviously, $a = 1$, $\varepsilon = 1$ in these units.

Our nanoparticle is constructed from an arrangement of pseudoatoms in a square lattice with a lattice constant b , which, in general, is not equal to the lattice constant a of the two planes. From this lattice we select those pseudoatoms whose distance from the cen-

ter of mass is smaller than the preset radius. In numerical simulations of Eq. (23), we focused on an approximately round crystalline nanoparticle with a radius of $5b$. The ‘‘commensurate’’ facets of the nanoparticle correspond to the rotational angle given by an integer multiple of $\pi/2$, $\phi_{comm} = n\pi/2$, whereas the ‘‘incommensurate’’ facets correspond to its half-integer multiple, $\phi_{incomm} = (n + 1/2)\pi/2$.

In our simulations, we have tried different values of b , and obtained qualitatively the same behaviour as for the $b = a = 1$ case reported below. As for other parameter values, we have taken the equilibrium distance of the Lennard-Jones potential (11) to be equal the lattice constant, $\sigma = 1$. The corrugation depth of the potential (12) was taken to be $\Delta U = 3/4$, and its decay length, as well as the decay length of the damping coefficient (14) were set to $\lambda = \xi = 1/5$. Finally, the spring constant was set to $\kappa = 1$, and the spring damping coefficient was $\eta_S = 10$. Other values of these parameters of a comparable order of magnitude produced qualitatively similar results.

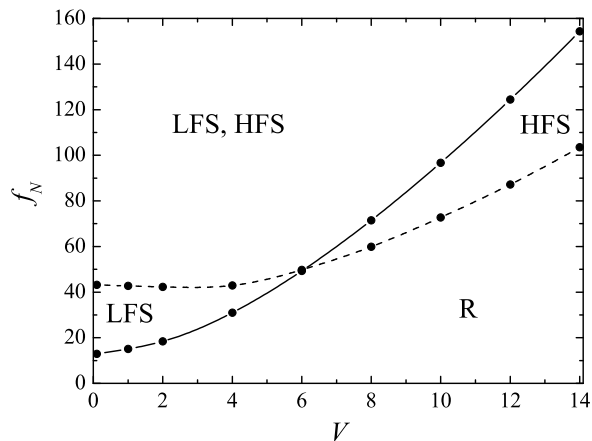


FIG. 2: State diagram of the system from Fig. 1 showing the stability regions of the low friction sliding (LFS), high friction sliding (HFS), and rolling (R) states.

B. State diagram

We have found that depending on normal load f_N and pulling velocity V , the nanoparticle can be rotating, or it can be stabilized in a sliding state of either low or high friction. The results of our numerical simulations are summarized in the state diagram of the system, Fig. 2, showing which friction regimes are stable for given values of f_N and V . When the normal load is sufficiently low, the nanoparticle can only exist in the rolling (R) state of motion, where the magnitude of the orientation angle steadily grows in time, as in Fig. 4(b). On the other hand, high normal load stabilizes the sliding state of mo-

tion, which can be either the low-friction sliding (LFS) or the high-friction sliding (HFS) state. In both these states, the orientation angle ϕ of the nanoparticle performs small rocking motion around the value, which is either $\pi/4$ (LFS state) or 0 (HFS state), up to an integer multiple of $\pi/2$. The LFS state corresponds to the incommensurate contact between the nanoparticle and the planes, while the high-friction sliding (HFS) state corresponds to the commensurate contact. The LFS state is stable above the solid line in Fig. 2, the HFS state above the dashed line. Above both separation lines, both LFS and HFS states are stable, and the actual state of motion of the nanoparticle depends on its initial preparation. Interestingly, to the left of the intersection point at ca. $V = 6$, there is a region at lower normal loads where the LFS state is the only stable state of motion; similarly, to the right of this point, there is a region at higher normal loads where the particle can exist only in the HFS state.

We now try to understand the state diagram from Fig. 2. In order to destroy the contact, work must be performed against the adhesion forces and the normal load. This work is done by the viscous drag, which scales linearly with the velocity V , and by the force generated by the moving corrugated potential. At low pulling velocities, it is the latter force that is responsible for breaking the contact. If the nanoparticle is in the LFS-state, the effective corrugation of the potential is lower than that in the HFS-state, because the contact is incommensurate and involves fewer atoms. Consequently, a smaller normal load is required to stabilize the LFS state, explaining its stability island in the low-velocity region.

At faster pulling, on the other hand, the effect of the potential corrugation becomes less important. This is so because the upper plane moves relatively fast with respect to the particle, so that the particle cannot follow the fast temporal variations of its potential and feels, instead of the true corrugation depth u_1 , a smaller time-averaged corrugation. Therefore, it is the viscous drag that is responsible for turning the nanoparticle at fast pulling. In order to break the contact, one has to overcome the adhesion between the nanoparticle and both planes. Since adhesion forces are larger in the HFS-state, smaller normal load is required to stabilize this state at fast pulling.

C. Friction force

Fig. 3 exemplifies the typical evolution of the friction force (2) in the three states. The curves (a) and (b) resemble the typical evolution of the friction force in an atomic friction experiment in the stick-slip regime^{24,25}. During the stick phases, the nanoparticle and the upper plane are almost stationary, while the elastic deformation of the spring attached to the top plane constantly increases due to pulling. When elastic energy becomes sufficient to initiate the slip, the nanoparticle gets dis-

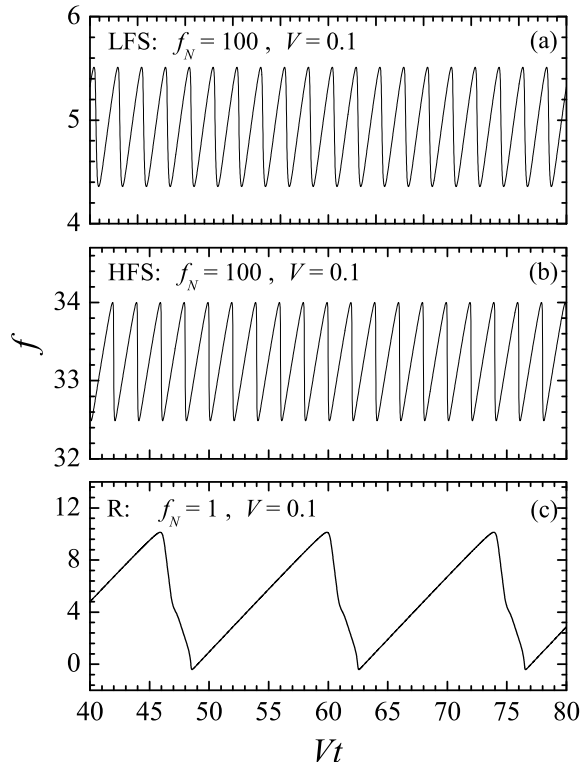


FIG. 3: Temporal evolution of the friction force (2) in (a) the LFS-state, (b) the HFS-state, and (c) the R-state. All curves are obtained for the same pulling velocity $V = 0.1$, but different normal loads: $f_N = 100$ for the curves (a) and (b), and $f_N = 1$ for the curve (c). The difference between the LFS- and HFS-curves (a) and (b) is in the orientation angle of the nanoparticle: namely, for the curve (a), the angle ϕ is close to $\pi/4$, and for the curve (b), it is close to zero.

placed in the x -direction by one lattice constant, and the upper plane by two lattice constants, see Eq. (22), resulting in a sudden relaxation of the spring. Consequently, the periodicity of the stick-slip curves in the LFS regime (a) and the HFS regime (b) equals two lattice constants. We note that the modulation amplitude of the stick-slip curves (a) and (b) is about the same, while the mean friction forces developed in both regimes are very different, in spite of the fact the pulling velocity and the normal loads are identical for the curves (a) and (b).

The curve (c) depicting the evolution of the friction force in the rolling state is interesting in three respects: its periodicity is notably larger than in the LFS- and HFS-cases (a) and (b); its modulation amplitude is also surprisingly high; the slope of the curve in a stick phase is much smaller than in the cases (a) and (b). These peculiarities can be explained as follows.

The periodicity of the “stick-roll” curve (c) is equal to the distance travelled by the upper plane during the “slip”²⁵. This distance is quite large, because the “slip”

event, seen as the sudden drop of the friction force, is associated not with the transition of the nanoparticle by one lattice constant, but with its rotation by an angle $\pi/2$ from one commensurate contact state to the next. During this rotation, the particle’s center of mass travels a distance of about $\pi R/2$. The actual distance is slightly smaller than this value, because the nanoparticle is not perfectly round. In view of Eq. (22), the periodicity of the curve (c) twice that value, that is, slightly smaller πR . For $R = 5$, this gives the periodicity that should be a bit smaller than 16 lattice constants. The periodicity of the curve (c) is indeed 14 lattice constants.

The second interesting feature is a roughly ten-fold larger amplitude of force variations in the rolling state compared to the LFS- and HFS-curves in Fig. 3, in spite of the fact that the normal load is two orders of magnitude smaller. As it turns out, the reason is precisely the much smaller normal load. In each stick phase, the elastic energy of the spring constantly builds up and is suddenly released to induce a rotation of the nanoparticle in the rolling state from Fig. 3 (c). At the same time, the nanoparticle in the stick phase can slightly turn and lift the top plane up against the small normal load. Since part of the torque applied to the particle by the spring is used to lift the upper plane, a much larger elastic force is necessary to induce the particle’s rotation, implying a large modulation amplitude of the curve in Fig. 3(c). For the curves from Fig. 3 (a) and (b), on the other hand, the normal load is too high to allow for any significant lifting of the upper plane, so that practically all of the force accumulated in the stick phase is used to initiate the slip.

Finally, the observed rate of force increase in the stick phase of the rotational regime (c) is much smaller than in the sliding regimes (a) and (b) for a similar reason. The rate of force increase in the stick phase is determined by an effective spring constant, κ_{eff} , which is given by a combination of the elasticity of the spring κ attached to the upper plane and the spring constant of the nanoparticle’s contacts with both planes, κ_{cont} . Since this “contact” spring is attached to the spring of the upper plane in series, the combination rule is $1/\kappa_{eff} = 1/\kappa + 1/\kappa_{cont}$, meaning that $\kappa_{eff} < \kappa_{cont}$. In view of the large difference in the normal load, the contact in the sliding regimes (a) and (b) is much more rigid than in the rolling regime (c). This implies a much smaller effective spring constant in the case (c) than in the cases (a) and (b), and a smaller rate of force increase.

Fig. 4 shows that in the rolling state, the shape of the force curve [Fig. 4(a)] can be quite different from the saw-tooth-like ones shown in Fig. 3. Here, the rotation angle [Fig. 4(b)] in the stick phase has the value $\phi = n\pi/2 + \pi/4$, meaning that the nanoparticle contacts the planes along its “incommensurate” facets. In the end of such a stick phase, the nanoparticle first quickly rotates by an angle of $\pi/4$ and enters another short-lived stick phase, where the contact is formed along the “commensurate” facets of the nanoparticle. Then, an-

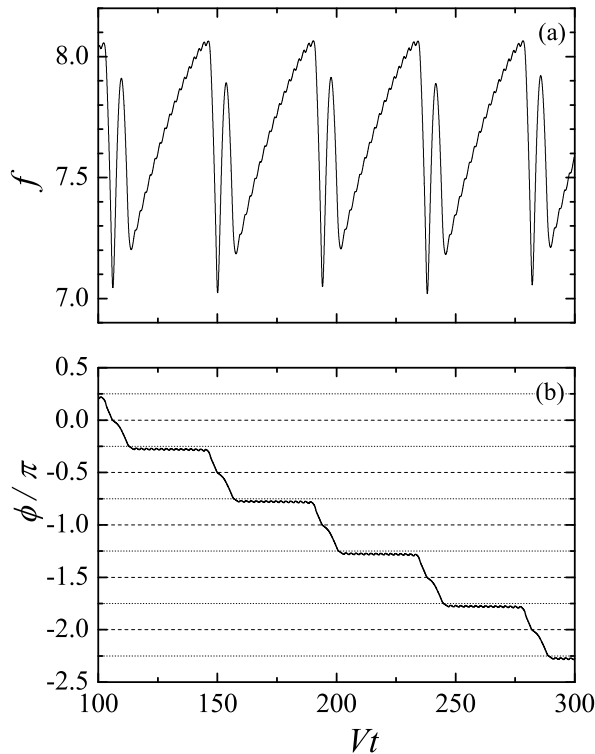


FIG. 4: Temporal evolution of (a) the friction force f from Eq. (2) and (b) the rotational angle ϕ in the rolling state corresponding to the pulling velocity $V = 4$ and normal load $f_N = 30$.

other rotation into an incommensurate state occurs, and the process repeats itself. As a result, the force evolution curve acquires an additional structure, with different stick phases corresponding to different particle-surface contacts. We note that the force curve observed in the carbon nanotube rolling experiments²⁰ also possesses a rather complex structure, presumably because of the variation of the contact properties of the nanotube “facets”.

D. Control of friction

The coexistence of the LFS and HFS states in Fig. 2 opens the possibility of switching between them by changing the control parameters, f_N and V . This process is illustrated in Fig. 5. Starting with the HFS-state within the coexistence region at $f_N = 100$ and $V = 2$, we reduce the normal load to $f_N = 30$ keeping the velocity constant, Fig. 5(a). This brings the system into that region of the state diagram from Fig. 2 where the LFS-state is the only stable one and induces a rotation of the nanoparticle by $\pi/4$. Restoring the normal load to its initial value brings the nanoparticle back into the

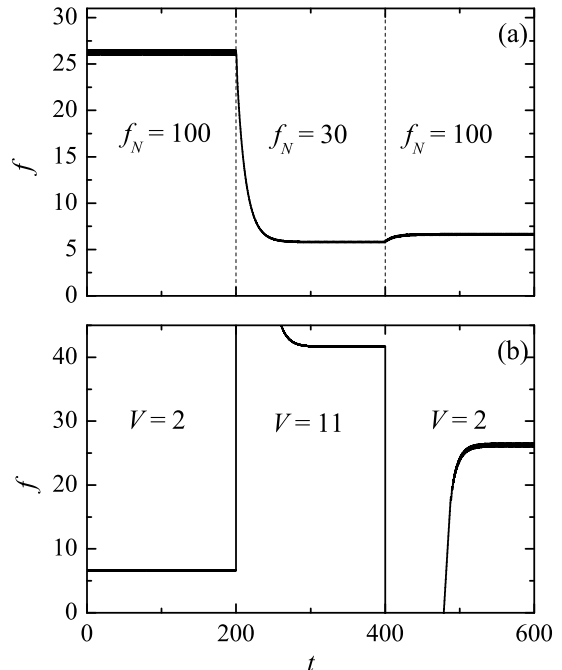


FIG. 5: Evolution of the friction force f from Eq. (2) during switching of the friction regime: (a) switching from HFS to LFS is performed by means of applying a negative pulse of the normal load at a constant velocity $V = 2$; (b) switching from LFS to HFS is achieved by applying a positive velocity pulse at a constant normal load $f_N = 100$.

coexistence region, but now its contact with both planes goes along the incommensurate sides.

In order to switch the nanoparticle back into the HFS state, one can increase the pulling velocity to a larger value, thus bringing the system out of the coexistence region into the HFS part of the state diagram, see Fig. 5(b). This results in a sudden stretching of the spring and, correspondingly, in a large spike of the elastic force. After the nanoparticles has rotated into the HFS configuration, the velocity is reduced to the initial value in the coexistence region of the state diagram. Again, this velocity reduction results in a sudden relaxation of the spring and in the large negative spike in the friction force. After that spike, the friction force stabilizes at a high value corresponding to the HFS-state of the system.

IV. CONCLUSIONS

To summarize, we have considered the rolling and sliding motion regimes of a cylindrical crystalline nanoparticle between two crystalline planes and found that the rolling state of motion is stable for sufficiently weak normal loads and fast pulling. An intriguing feature of the state diagram from Fig. 2 is the existence of the stability

island of the LFS state, where the contact between the nanoparticle and the planes is incommensurate. This is in striking contrast with the finding of Refs. 14,15, where the HFS commensurate state was the only stable one. The reason for this difference is that, in the works 14,15, the flat nanoparticle was rotating around the axis perpendicular to the planes, while in our work, the rotation axis is parallel to the planes and perpendicular to the direction of motion. We have shown that using nanoparticles as a lubricant, one can achieve either low or high friction at the same values of normal load and pulling velocity. This finding is at variance with the results from Refs. 2–4, where adjustment of these parameters was essential for friction control, so that different friction regimes could be realized only for different values of V and f_N .

Even though the results reported in this paper have been obtained for the special case of equal lattice constants of the nanoparticle and the planes, we have found qualitatively similar behaviour also in the case of unequal lattice constants. The fact that some facets of the nanoparticle are commensurate or incommensurate with the surfaces facilitates the discussion of the results, but is not central for the physical mechanism underlying the friction states of the nanoparticle. What is important is that different facets of the nanoparticle are characterized by different interaction energies with the surfaces. If this condition is fulfilled, then several sliding states and the rolling state can be realized, even when all facets are incommensurate with the surfaces, or if they are commensurate, but differ in the number of contact atoms.

In our analysis, several important effects have been neglected, such the nanoparticle's possible asymmetry, inertia effects, and the effect of thermal noise. All these effects, when properly taken into account, may lead to qualitatively new friction regimes. In particular, nanoparticles of other shapes can exhibit different state diagrams and, correspondingly, can allow for different

friction switching mechanisms. For instance, if the nanoparticle is asymmetric, it can stick to one plane and slide against the other; or it can slide with respect to both planes, but with the velocity very different from half the velocity of the upper plane. Next, the effects of thermal noise are typically negligible compared to load and interaction forces. However, in the systems where noise effects play a significant role, the nanoparticle is expected to spontaneously perform thermally induced transitions between the LFS and the HFS states within the coexistence region, so that higher normal loads would be required to stabilize them. In this case, one can expect the appearance of new regions in the state diagram, where friction is controlled by thermal noise. Finally, inertia introduces new characteristic time scales into the problem – the inverse resonance frequencies of the nanoparticle's vertical, horizontal, and angular oscillations within the potential of the two surfaces. If the time of pulling by one lattice constant, a/V , becomes comparable to any of these time scales, new friction regimes associated with the nanoparticle's resonant motion can be expected. Exploring new friction regimes related to these and possibly other factors can be an exciting subject for future research, both theoretical and experimental.

V. ACKNOWLEDGEMENTS

We thank the Deutsche Forschungsgemeinschaft (Collaborative Research Center SFB 613) and the ESF programs NATRIBO and FANAS (collaborative research project Nanoparma – 07-FANAS-FP-009) for financial support.

* E-mail:mykhaylo@physik.uni-bielefeld.de

¹ R. Feynman, *There's plenty of room at the bottom*, Caltech Eng. Sci. **23**, 22 (1960).

² A. Socoliuc, R. Bennewitz, E. Gnecco, and E. Meyer, Phys. Rev. Lett. **92**, 134301 (2004).

³ S.Y. Krylov, K.B. Jinesh, H. Valk, M. Dienwiebel, and J.W.M. Frenken, Phys. Rev. E **71**, 065101(R) (2005).

⁴ A. Socoliuc, E. Gnecco, S. Maier, O. Pfeiffer, A. Baratoff, R. Bennewitz, and E. Meyer, Science **313**, 207 (2007).

⁵ K.E. Drexler, *Nanosystems: Molecular Machinery, Manufacturing and Computation* (New York, Wiley, 1987).

⁶ R.C. Merkle, Nanotech. **4**, 86 (1993).

⁷ M. Hirano and K. Shinjo, Phys. Rev. B **41**, 11837 (1990); Surf. Sci. **283**, 473 (1993); M. Hirano, K. Shinjo, R. Kaneko, and Y. Murata, Phys. Rev. Lett. **67**, 2642 (1991); Phys. Rev. Lett. **78**, 1448 (1997).

⁸ G.S. Verhoeven, M. Dienwiebel, and J.W.M. Frenken, Phys. Rev. B **70**, 165418 (2004).

⁹ M.H. Müser, M. Urbakh, and M.O. Robbins, Adv. Chem.

Phys. **126**, 187 (2003).

¹⁰ M.H. Müser, EPL **66**, 97 (2004).

¹¹ J.S. Ko and A.J. Gellman, Langmuir **16**, 8343 (2000).

¹² J.M. Martin, C. Donnet, Th. Le Mogne, and Th. Epicier, Phys. Rev. B **48**, 10 583 (1993).

¹³ M. Dienwiebel, G.S. Verhoeven, N. Pradeep, J.W.M. Frenken, J.A. Heimberg, and H.W. Zandbergen, Phys. Rev. Lett. **92**, 126101 (2004).

¹⁴ Ph. Depondt, A. Ghazali, and J.-C.S. Lévy, Surf. Sci. **419**, 29 (1998).

¹⁵ A.E. Filippov, M. Dienwiebel, J.W.M. Frenken, J. Klafter, and M. Urbakh, Phys. Rev. Lett. **100**, 046102 (2008).

¹⁶ O.M. Braun, Phys. Rev. Lett. **95**, 126104 (2005); O.M. Braun and E. Tosatti, J. Phys.: Cond. Matt. **20**, 354007 (2008); Phil. Mag. Lett. **88**, 509 (2008).

¹⁷ S.B. Legoas, R. Giro, and D.S. Galvão, Chem. Phys. Lett. **386**, 425 (2004).

¹⁸ J.W. Kang and H.J. Hwang, Nanotechnology **15**, 614 (2004).

- ¹⁹ C. Ritter, M. Heyde, U.D. Schwarz, and K. Rademann, *Langmuir* **18**, 7798 (2002).
- ²⁰ M.R. Falvo, R.M. Taylor II, A. Helsen, V. Chi, F.P. Brooks Jr., S. Washburn, and R. Superfine, *Nature* **397**, 236 (1999).
- ²¹ M.R. Falvo, J. Steele, R.M. Taylor II, and R. Superfine, *Tribol. Lett.* **9**, 73 (2000).
- ²² M. Evstigneev and P. Reimann, *Phys. Rev. B* **82**, 224303 (2010).
- ²³ L.D. Landau, E.M. Lifshitz, and L.P. Pitaevskii, *Statistical Physics* (Oxford, Pergamon Press, 1980).
- ²⁴ C.M. Mate, G.M. McClelland, R. Erlandsson, and S. Chiang, *Phys. Rev. Lett.* **59**, 1942 (1987).
- ²⁵ M. Evstigneev, A. Schirmeisen, L. Jansen, H. Fuchs, and P. Reimann, *Phys. Rev. Lett.* **97**, 240601 (2006).